Author/s:
Mazaheri, O;Lin, Z;Xu, W;Mohankumar, M;Wang, T;Zavabeti, A;McQuillan, RV;Chen, J;Richardson, JJ;Mumford, KA;Caruso, F

Title:
Assembly of Silicate–Phenolic Network Coatings with Tunable Properties for Controlled Release of Small Molecules

Date:
2024-12-27

Citation:
Mazaheri, O., Lin, Z., Xu, W., Mohankumar, M., Wang, T., Zavabeti, A., McQuillan, R. V., Chen, J., Richardson, J. J., Mumford, K. A. & Caruso, F. (2024). Assembly of Silicate–Phenolic Network Coatings with Tunable Properties for Controlled Release of Small Molecules. Advanced Materials, 36 (52), https://doi.org/10.1002/adma.202413349.

Persistent Link:
https://hdl.handle.net/11343/354463

Assembly of Silicate–Phenolic Network Coatings with Tunable Properties for Controlled Release of Small Molecules

*Omid Mazaheri, Zhixing Lin, Wanjun Xu, Mirudula Mohankumar, Tianzheng Wang, Ali Zavabeti, Rebecca V. McQuillan, Jingqu Chen, Joseph J. Richardson, Kathryn A. Mumford, and Frank Caruso**

O. Mazaheri, Z. Lin, W. Xu, M. Mohankumar, T. Wang, A. Zavabeti, R. V. McQuillan, J. Chen, K. A. Mumford, F. Caruso
Department of Chemical Engineering, The University of Melbourne, Parkville, Victoria 3010, Australia
E-mail: fcaruso@unimelb.edu.au

O. Mazaheri, Z. Lin, R. V. McQuillan, K. A. Mumford, F. Caruso
ARC Research Hub for Smart Fertilisers, The University of Melbourne, Parkville, Victoria 3010, Australia
E-mail: fcaruso@unimelb.edu.au

A. Zavabeti, J. J. Richardson
Department of Chemical Engineering, RMIT University, Melbourne, Victoria 3001, Australia

Keywords: controlled release urea, hydrophobic effect, metalloid–organic frameworks, silicate–phenolic networks, silicon

Engineered coatings are pivotal for tailoring the surface properties and release profiles of materials for applications across diverse areas. However, developing robust coatings that can both encapsulate and controllably release cargos is challenging. Herein, a dynamic covalent coordination assembly strategy is used to engineer robust silicate-based coatings, termed silicate–phenolic networks (SPNs), using sodium metasilicate and phenolic ligands (tannic acid, gallic acid, pyrogallol). The coatings are pH-responsive (owing to the dynamic nature of the covalent bonding), and their hydrophobicity can be tuned upon their post-functionalization with hydrophobic gallates (propyl, octyl, lauryl gallates). The potential of the SPN coatings for the controlled release of small molecules, such as urea (a widely used fertilizer), is

demonstrated—controlled release of urea in soil is achieved in response to different pHs (up to 7 days) and different hydrophobicity (up to 14 days). Furthermore, leveraging the presence of silicon (within the coating) and post-functionalization of the SPN coatings with metal ions (Fe^{3+}, Cu^{2+}, Zn^{2+}) generates a multipurpose delivery system for the sustained release of micronutrient fertilizers, silicon and metal ions, over 28 and 14 days, respectively. These SPN coatings have potential applications beyond agriculture, including nutrient delivery, separations, food packaging, and medical device fabrication.

1. Introduction

Supramolecular metal–organic coatings have received considerable interest owing to their hybrid and controllable physiochemical properties stemming from the metal ions and organic ligands.[1,2] For example, metal–phenolic networks (MPNs) have emerged as versatile conformal coatings applicable to nearly any substrate owing to the highly adherent nature of polyphenols and their ability to interact with various materials through diverse supramolecular interactions, including hydrogen bonding, metal coordination, and π–π and hydrophobic interactions. The rapid coordination between the catechol groups of phenolic ligands and metal ions enables the formation of MPN coatings within seconds. However, such rapid kinetics of complexation often limits control over the growth and thickness of the coatings, which can cause challenges for some applications such as the controlled delivery and release of small water-soluble molecules.[3,4] Controlling the supramolecular assembly of polyphenol-based coatings offers a route to slow the reaction kinetics and thereby allowing for control over the physiochemical properties of the coatings either by controlling the pore size or modulating the coating growth.

The introduction of silicon (element) in the assembly may offer a route to control the kinetics of coordination and to engineer coatings with advanced functionalities. Catechols can depolymerize SiO_2—a component of silicates with an ionic structure such as orthosilicate SiO_4^{4-}, metasilicate SiO_2^{3-}, and pyrosilicate $Si_2O_6^{7-}$—via coordination by forming bis and tris(catecholate)silicate dianions, as discovered in 1951.[5] Since then, the structures of catecholate silicate complexes have been widely investigated,[6-17] and recently a variety of crystalline silicate–organic frameworks have been developed.[18-21] However, the formation of robust uniform coatings using catecholate silicate complexes is challenging as high ionic strength originating from salts can cause aggregation of the precursors.[22] Moreover, using a low silicic acid-to-phenolic ligand molar ratio (i.e., <0.1) makes it

challenging to determine whether the coating consists of uniformly connected catecholate silicate complexes or simply phenolic aggregates and separate silicate structures.[23,24]

Herein, we introduce a dynamic covalent assembly strategy to engineer functional silicate–phenolic network (SPN) coatings using sodium metasilicate and a library of naturally abundant phenolic ligands (**Scheme 1**), including tannic acid (TA), gallic acid (GA), and pyrogallol (PG) (Figure S1). In situ studies of mixtures of sodium metasilicate and phenolic ligands in aqueous solutions suggest the dynamic assembly of catechol moieties with tetra and hexahedral dianionic SiO_x building blocks via covalent bonding, which can be tailored by aging time, concentration and precursor ratio, to form catecholate silicates complexes. In contrast to a previous study,[22] no particles are generated in solution owing to the low reactivity of Si–catechol (stability constant, log $K_1 \sim -11.5$),[25] which hinders spontaneous coordination and subsequent particle growth. The gradual breakdown of oligomeric metasilicate anion structures, which is facilitated by the catechol moieties, leads to the assembly and growth of stable and amorphous SPN coatings on different substrates (i.e., urea granules, planar gold, and polystyrene nanoparticles) with thickness coatings ranging from the nano to micrometer scale. Notably, the SPNs show pH responsiveness owing to the dynamic nature of the covalent bonding, enabling their disassembly in both acidic (pH < 5) and alkaline (pH > 10) solutions, which can be potentially applied in response to environmental stimuli. The SPN coating can be further functionalized with hydrophobic gallates (HGs; i.e., propyl gallate (PrG), octyl gallate (OG), and lauryl gallate (LG)) (Figure S1). Moreover, our study provides a paradigm for designing tunable hydrophobic coatings to engineer the controlled release of small molecules, such as urea, with molecular dimensions of <0.5 Å, for potential application in the agricultural sector, allowing controlled release of urea up to 14 days. Furthermore, by leveraging the incorporation of silicon within the SPNs and post-functionalization of the SPN coatings with micronutrients (i.e., Si^{4+}, Fe^{3+}, Cu^{2+}, and Zn^{2+}), we can engineer a versatile multipurpose delivery system that displays sustained release of micronutrient fertilizers over 28 days. Tuning the urea release offers the potential to boost availability and minimize fertilizer use in large-scale crop planting, leading to more sustainable agricultural practices and lower environmental footprints.

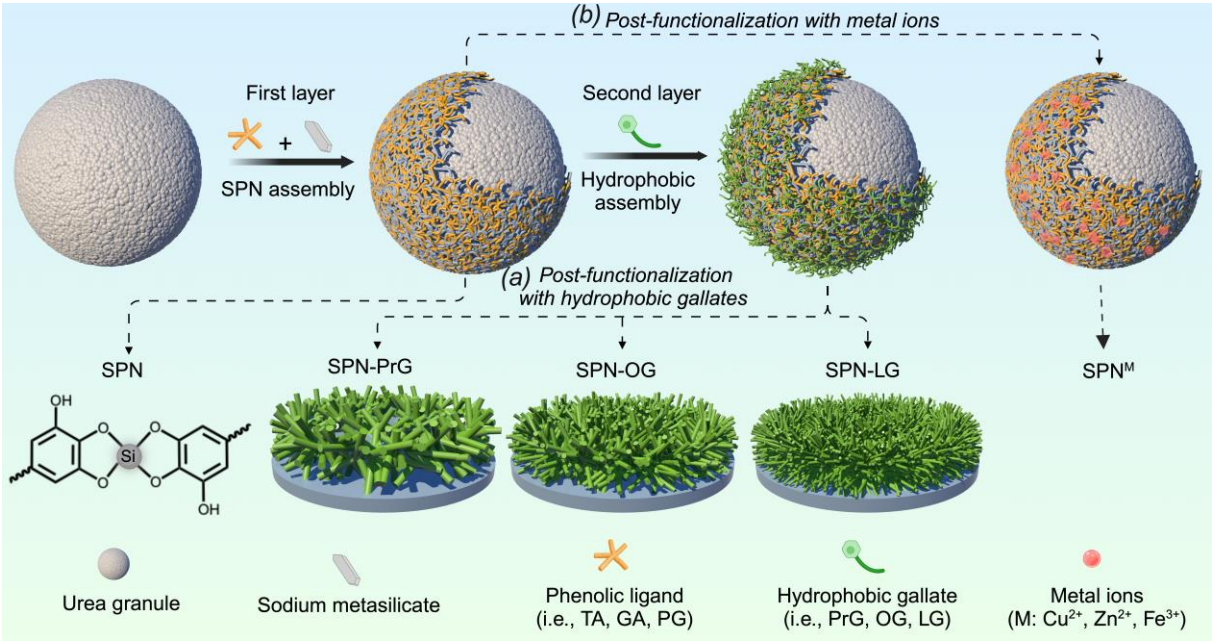

Scheme 1. Schematic of the assembly of an SPN coating on a urea granule (urea@SPN), and post-functionalization of the SPN coating with (a) hydrophobic gallates to engineer hydrophobic SPN coatings (SPN-PrG, SPN-OG, SPN-LG) or (b) metal ions to engineer SPN^M coatings (where M is the metal ion). The scheme was partially created using BioRender.

2. Results and Discussion

2.1. Assembly of SPNs in Solution

We first investigated the mechanism of Si–TA covalent bonding by mixing TA and sodium metasilicate in aqueous solutions (**Figure 1**). The Si–TA solution gradually transitioned from blue to yellow over 10–15 min after the addition of the sodium metasilicate solution to the TA solution (Figure 1a), and no precipitation was detected, as determined by dynamic light scattering (data not shown). In situ wide-angle X-ray scattering (WAXS) measurements revealed the kinetics of the assembly process (Figure 1b), wherein the broad peak at ~2.4 $Å^{-1}$ could be attributed to O–Si–O of SiO_4 tetrahedrons[26] and the peak at 0.1 $Å^{-1}$ that gradually increased over time was likely due to the gradual formation of extended bis and/or tris complexes. Likewise, the UV–vis spectra of the Si–TA solution suggested a dynamic covalent bonding system over time, particularly with extended aging. Dynamic covalent bonding refers to reversible covalent bonds that can cleave and reform spontaneously or in response to stimuli such as pH and temperature. Within the first 10 min, an absorption band appeared within the range of ~500–800 nm with λ_{max} of 625 nm, indicating the formation of mono/bis Si–TA complexes (Figure 1c and Figure S2). As time progressed (10–360 min), the intensity

of that peak decreased while a new peak at 450 nm appeared and its intensity increased with aging time (Figure 1d), indicating the transition from mono/bis to bis/tris complexes over time. No significant changes were observed in the UV–vis spectra below 400 nm (Figure S3). When sodium metasilicate reacts with water, it undergoes hydrolysis to produce $Si(OH)_4$ and NaOH, resulting in an increase in the pH of the solution.[27] In the presence of TA, we noticed a gradual decrease in the pH of the solution mixture by ~0.5–1 pH unit (depending on the Si-to-TA ratio and concentration), which was consistent with the observed color changes, likely due to the deprotonation of TA by NaOH. These results collectively suggest that the Si–TA complexes undergo conformational changes with time, which allows for bridging between complexes in solution to form extended bis and tris structures for up to 16 h (Figure S4). The UV–vis spectra of the Si–TA solution revealed a new peak at 360 nm with increasing Si:TA molar ratios (Figure 1e). As the oxidation of TA to quinone intermediates occurs at 325 nm at high pH values (Figure S5), this suggested that an in situ increase in the NaOH concentration could enhance the likelihood of oxidation of the catechol moieties to form quinone-based Si–TA complexes.[16,28,29] The proportion of the mono-, bis-, and tris-coordination species at different Si:TA molar ratios (i.e., 1:1 to 5:1) was determined by Gaussian peaks fit to the UV–vis spectra (Figure S6). Specifically, the coordination of the tris-state was predominant at a Si:TA ratio of 1:1, whereas the proportion of mono- and bis-states increased when the ratio increased to 5:1.

To understand the structure of the complexes, we studied Si–GA complexes in solution at different molar ratios and pH over time by liquid chromatography–mass spectrometry in negative ion mode (Figures S7–S14). GA was chosen because of its simple structure. The two main peaks at retention times of 1.6 and 2 min were assigned to Si^{4+} species and Si–GA complexes, respectively. Increasing the Si:GA ratio from 0.2:1 to 5:1 resulted in an increase in the abundance of Si–GA complexes within the molecular weight (M_w) range of 300–2000, indicating the formation of larger complexes within the solution. It is difficult to identify specific complex structures owing to the myriad of possibilities such as mono-, bis-, tris-, quinone, μ-oxo bridging, and μ-catechol bridging (Figure 1f).[3,30] Oligomeric $–SiONa^+$ species (*m*/*z* 68) within the M_w of 200–2000 were observed. Initially, the abundance of these species increased as the Si:GA ratio increased from 0.2:1 to 1.5:1 and subsequently decreased as the Si:GA ratio further increased to 5:1. Furthermore, changing the Si:GA ratio from 0.2:1 to 5:1 resulted in a change in the pH from 4 to 12, suggesting that the oligomeric $–SiO_x$ species undergo hydrolysis at a relatively high or low Si:GA molar ratio. Moreover, Si–GA

complexes were not detected when the pH of the Si–GA solution (Si:GA molar ratio 1.5:1) was adjusted to 2.5 or 8 using HCl; this is likely due to the reaction between HCl and silicate structure causing the catecholate silicate complex to cleave.[31]

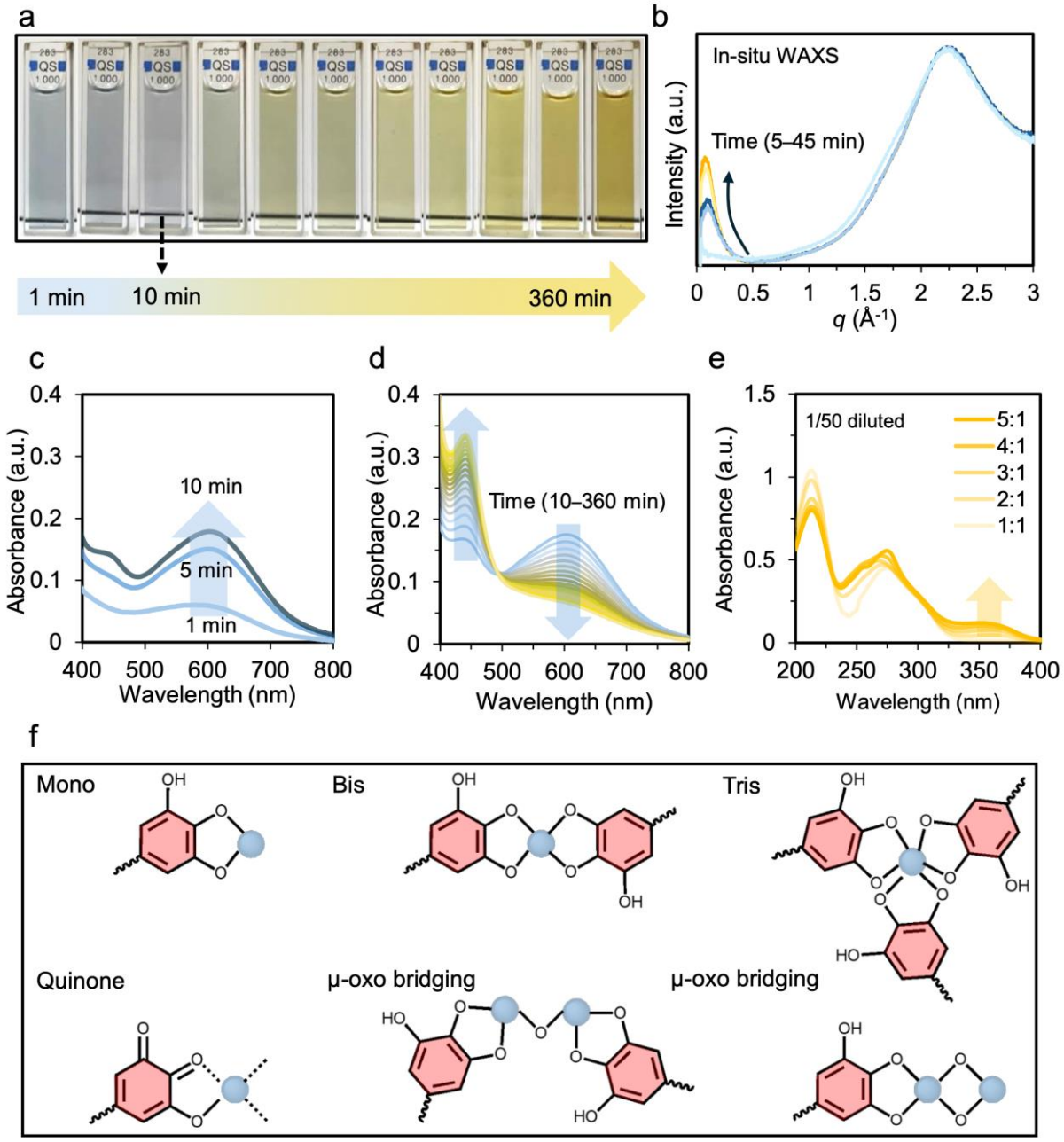

Figure 1. Assembly of SPNs in solution. (a) Photograph of Si–TA solutions showing color changes as a function of solution aging time. (b) In situ growth of catecholate silicate complexes as measured by WAXS. UV–vis spectra of Si–TA solutions at (c, d) different aging times and (e) different Si:TA molar ratios after 2 h of aging. (f) Possible structures of catecholate silicate complexes in solution (the ionic charge and counterions are not shown for simplicity).

2.2. Chemistry and Coordination of SPN Coatings

We further explored the formation of SPN coatings, using a mixture of TA and sodium metasilicate in aqueous solution, on different substrates including planar Au, polystyrene nanoparticles, and urea granules (**Figure 2**). Quartz crystal microbalance (QCM) measurements demonstrated a significant frequency shift (Δf), due to a mass change, upon growth of the coating on the Au substrate, whereby SPNs grew continuously over 30 min (Figure 2a). The difference in Δf before coating and after washing indicated the formation of stable SPNs. Changing the pH of the solution from 8 to 4 or 10 led to smaller Δfs from 20 to 7 and 14, respectively. This may be due to either increased electrostatic repulsions between the substrate and Si–TA complexes or a decreased likelihood of complex formation at these pH levels (Figure 2b and Figure S15). Stable SPN coatings were observed on polystyrene nanoparticles by scanning electron microscopy (SEM; Figure S16a) with a thickness of 25 nm as determined by atomic force microscopy (Figure S16b,c). Comparison of the Raman spectra of sodium metasilicate and the SPN coating (Figure 2c) revealed distinct differences between the pristine silicate structure and its coordinated form with TA. The Raman spectrum of sodium metasilicate could be divided into three main characteristic spectral regions, i.e., 300–550, 700–800, and 800–1000 cm^{-1}. These spectral regions can be respectively assigned to bridging and nonbridging Si–O–Si bonds for four- and six-member ring vibrations, bending vibrations of chain and ring in both crystalline and amorphous form, and stretching vibrations of tetrahedral SiO_4.[32] After the configuration changes in SiO_2 and coordination of Si^{4+} with TA, the intensity of these peaks significantly decreased and a broad peak at 500–600 cm^{-1} emerged, which was attributed to Si–O vibration arising from Si–galloyl coordination (Figure 2c). These findings suggest that though sodium metasilicate powder, as the source of Si used in this work, is crystalline, its incorporation with polyphenols such as TA leads to the formation of amorphous coatings. Si–TA coordination was further supported by the Si–O asymmetric stretching vibration observed at 670 cm^{-1} in the Fourier transform infrared (FTIR) spectrum of the SPN coating (Figure S17).[33] The intensity of the bands observed at 1017 and 1170 cm^{-1} in TA decreased in the SPN coating, while a strong band appeared at 1063 cm^{-1} in the SPN coating. As these bands have large contributions from C–O and C–C vibrations, the interaction of Si^{4+} with phenolic groups led to a decrease in intensity of these two peaks. The bands at 1650 and 1560 cm^{-1} in the SPN coating are associated with the ester group in TA.[24,34] These bands underwent a large shift upon complexation, further supporting the interaction of Si^{4+} with an ester group. The X-ray photoelectron spectroscopy (XPS) pattern of Si^{4+} in the SPNs showed a binding energy shift from 101.6 to 103.5 eV compared to

sodium metasilicate, which can be assigned to the octahedral coordination of Si^{4+} with TA (likely bis-structure) (Figure S18).[35] A high degree of crystallinity in the silica source was revealed by X-ray diffraction, whereas the SPN coatings were amorphous, confirming the geometry changes of SiO_4 upon coordination with TA and in accordance with what is generally observed for MPNs (Figure S19).[36] Owing to its robust structure, the SPN coating displayed higher resistance to thermal decomposition than pristine TA as indicated by thermogravimetric analysis. The thermogram of TA revealed two significant mass losses at 250 and 310 °C, related to breaking of ester and C–C bonds, whereas a higher temperature of at least 420 °C was required to induce a notable mass loss in SPNs (Figure S20).[37]

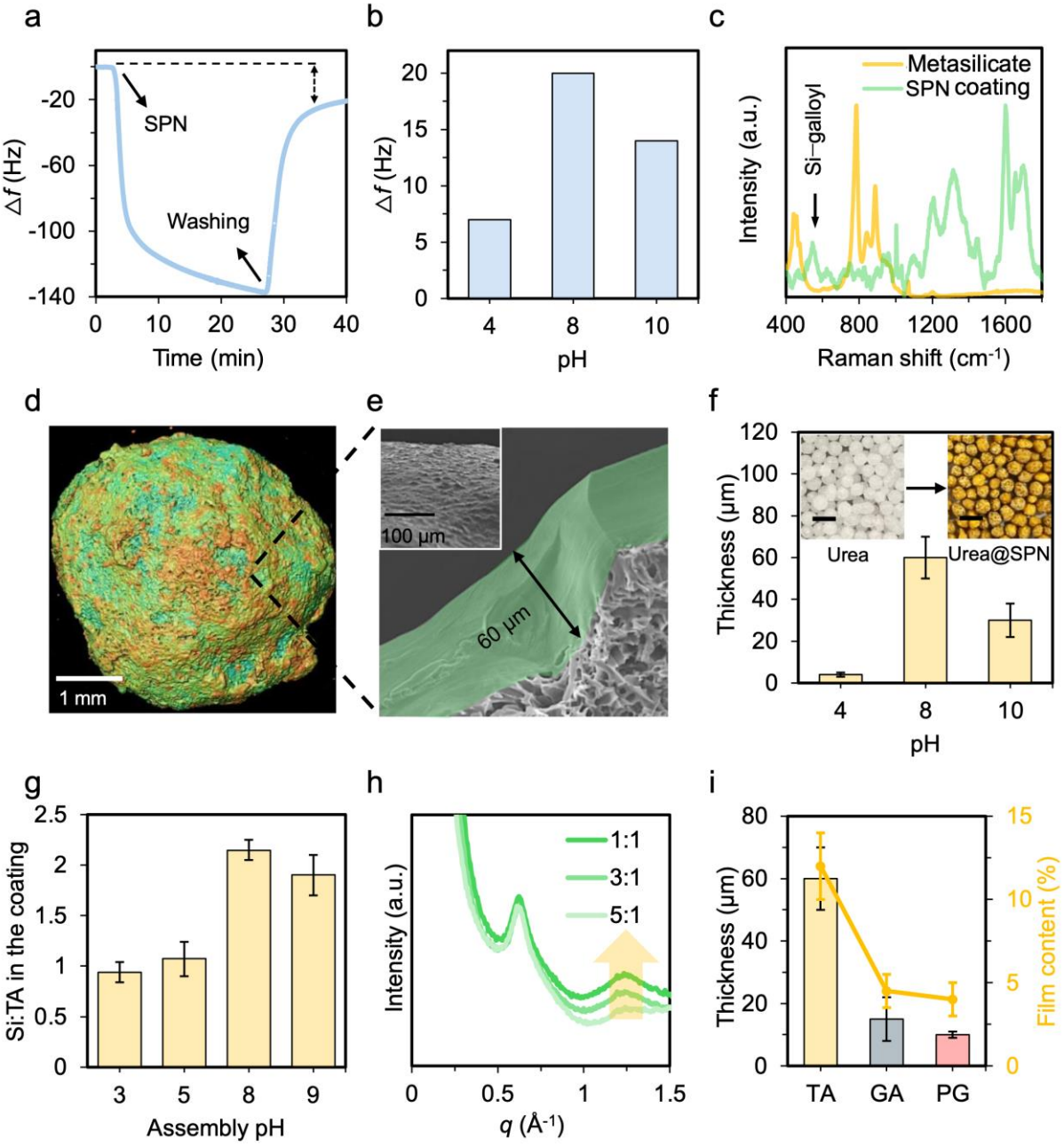

Figure 2. Assembly of SPN coatings. (a) Deposition of an SPN coating (on planar Au), as monitored by QCM. (b) Frequency shifts upon SPN coating formation using precursor solutions at different pHs. (c) Raman spectra of an SPN coating and sodium metasilicate. (d) Micro-CT image of an SPN coating on a urea granule. The normalized color map indicates the relative density of the coatings, with red representing higher density, green medium density, and blue lower density. (e) False colored cross-section image (original included image in Figure S21d) and surface image (inset) of urea@SPN. False-colored processing was performed to facilitate distinction between the coating and the substrate (urea granule). (f) Thickness of SPN coating on urea (urea@SPN) prepared at different pH values and photographs of urea granules and urea@SPN (insets). Scale bars are 5 mm. (g) Changes in Si:TA molar ratio of SPN coatings assembled at different pH values. (h) WAXS spectra of SPN coatings assembled at different molar ratios of Si:TA. (i) Thickness of SPN coatings assembled on urea granules with different phenolic ligands, as measured by SEM, and the coating content in the urea@SPN samples (yellow line). The SPN coatings on urea granules were obtained after 10 deposition steps using a solution with a Si:TA molar ratio of 3:1 and pH 8, unless mentioned otherwise. Data are shown as the mean ± standard deviation, with three specimens being analyzed for each sample, where applicable.

A multistep deposition on urea granules was then performed to further explore the potential of SPNs for the controlled release of urea in agricultural applications. The micro-computed tomography (CT) image of SPN-coated urea granules (urea@SPN) confirmed the formation of relatively uniform coatings (Figure 2d). The surface and cross-section images of the SPN coatings prepared at a Si:TA molar ratio of 2:1 showed a relatively smooth surface with a thickness of ~60 μm (Figure 2e). The thickness was tuned by the number of deposition steps employed (i.e., from 4 to 60 μm for up to 10 deposition steps, with each step involving the application of 0.1 mL of Si–TA solution, totaling 1 mL) (Figure 2f (insets) and Figure S21). The thickness of the coatings decreased when an acidic (pH 4) or an alkaline (pH 10) stock Si–TA solution was used. For example, at pH 4, the thickness reduced significantly to ~3–5 μm and at pH 10, it decreased to ~35 μm for 10 deposition steps (Figure 2f and Figure S22), which agrees with the QCM results. Inductively coupled plasma (ICP)/UV–vis spectroscopic measurements of digested coatings in acid indicated that changes in the pH and Si:TA molar ratio could lead to different chelation states and silicon content in the coatings (Figure 2g and Figure S23 and S24).[4] WAXS measurements of the coatings prepared using different Si:TA molar ratios revealed that the intensity of the peak between 1.0–1.5 $Å^{-1}$ decreased when the

Si:TA ratio increased from 1:1 to 5:1, likely indicating the formation of μ-oxo bridges in the complexes (Figure 2h).[38] The broad profile of this peak, along with the lack of any distinct sharp peaks in the WAXS spectra of the SPN coatings, suggests that no crystalline structure is generated through the formation of catecholate silicate complexes. SPN coatings were also assembled using GA and PG, confirming the versatility of the system (Figure 2i and Figure S25). However, more stable and thicker coatings were obtained when TA was used as opposed to GA and PG (which led to reduced SPN coating thicknesses), likely due to the higher number of catechol sites provided by TA compared to GA and PG.

2.3. Stability of SPN Coatings

We next investigated the stability of the SPN coatings by incubating hollow SPN capsules in a range of solutions (**Figure 3**) including water (ambient temperature and 85 °C), ethylenediaminetetraacetic acid (EDTA, 100 mM), Tween 20 (100 mM), urea (100 mM), tetrahydrofuran (THF), dimethylformamide (DMF), and sodium chloride (NaCl, 100 mM) (Figure 3a, Figure S26). The capsules were obtained following removal of urea from urea@SPN. The SPN coatings displayed high stability in THF and DMF, highlighting the presence of covalent coordination in the Si–TA complexes rather than π–π stacking between Si^{4+} and galloyl moieties. In contrast, the coatings readily disassembled in water (65%), urea (90%), and Tween (100%) within 2 weeks of incubation, likely due to the hydrolysis of the silicate structure. Rapid dissociation of the SPN coatings was observed when the coatings were incubated in water at 85 °C, implying the thermodynamic covalent coordination of Si–galloyl. The SPN coatings demonstrated greater stability in EDTA and NaCl than in water, showing only 10% and 5% disassembly, respectively, over a two-week period. The difference in the coordination chemistry between catechols and silicate may explain the observed relatively higher stability of SPNs when compared with MPNs upon the addition of EDTA. The coordination chemistry in MPNs relies on complex coordination between metals and catechols, whereas the coordination between silicate and catechols involves dynamic covalent bonding,[6] which forms relatively stronger bonds than complex coordination. Additionally, the change in color of the SPN coatings from light brown to dark brown suggests the formation of SPNs with different structural characteristics. Therefore, rather than acting as a dissociating agent, EDTA might participate in coordination involving μ-oxo and μ-catechol bridging with the silicate structure, contributing to the formation of more robust SPN coatings and hindering hydrolysis.[39] Likewise, Na^+ can impact the dissociation constant of SPNs through an increase in the ionic strength of the solution.[40] We further investigated the

stability of coatings prepared using different Si:TA molar ratios and different pH levels (Figure S27). The coatings prepared using Si:TA ratios varying between 2:1 and 4:1 were stable after 1 week, whereas those prepared using Si:TA ratios of 5:1 and 1:1 disintegrated within 1 day. Coatings prepared at pH levels of 8.2 and 9.2 disassembled by 35% and 45% within 1 week, respectively, whereas the coatings prepared at pH < 5 disintegrated after 6 h.

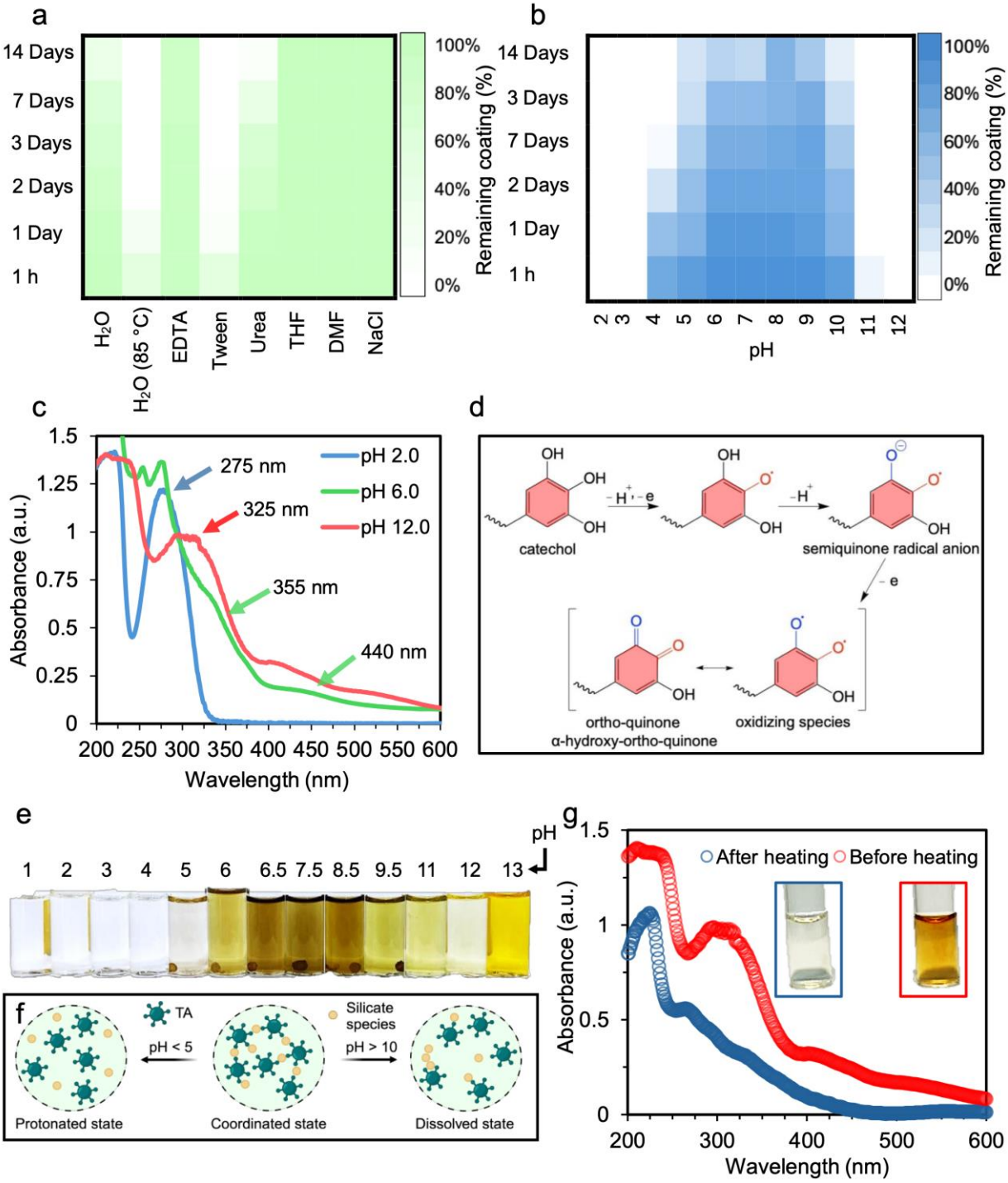

Figure 3. Stability of SPN capsules (after removal of urea granules). (a, b) Heat maps showing the percentage of SPN coating remaining after incubation in (a) different media or

(b) different pH solutions over 14 days. (c) UV–vis spectra of SPN coatings incubated in water at different pH values. (d) Mechanism of the oxidation of catechol groups to quinone species. (e) Dual pH responsiveness of SPN coatings incubated in different pH solutions for 7 days. (f) Schematic representation of SPN states at different pH values. (g) UV–vis spectra of SPN coatings incubated in water at pH 12 before and after heating at 90 °C (inset shown photographs of the solutions). Figure 3f was created using BioRender.

These results indicate that the coatings exhibit dual pH responsiveness—they completely disassembled at pH < 5 and pH > 10 but were more stable at pH 8, with 30% disassembly observed after 2 weeks (Figure 3b). UV–vis spectroscopy of the solutions following the disassembly of SPNs at pH 6 revealed an absorbance band at 355 and 440 nm, confirming the coordinated state of Si–TA in solution after incubation. In contrast, the UV–vis spectra of the disassembled SPNs appeared comparable at pH values of 2 and 12 (Figure 3c), indicating that free TA molecules or quinone intermediate species were predominant at these pH values. Particularly, the absorbance peak at 275 nm for the sample incubated at pH 2 indicated the presence of protonated hydroxyl groups of catechol. As the pH increased to 12, this peak shifted to 325 nm, suggesting the formation of quinone intermediates,[28] where the oxidation of the catechol groups of TA by nucleophilic entities can lead to the formation of *ortho*-quinones and/or α-hydroxy-*ortho*-quinones (Figure 3d).[41] The absorbance bands related to Si–TA coordination were still detectable even after coating disassembly. The color of the solutions was also dependent on the pH, i.e., transparent at pH < 5, dark brown at 5 < pH <10, and yellow–orange at pH > 10 (Figure 3e). At high pHs (e.g., pH > 9.5), the disassembly of Si^{4+} complexes, such as μ-oxo bridged polymeric Si^{4+} species, occurs due to hydrolysis,[42] and the dissolved Si^{4+} and TA intermediates can then freely undergo configuration rearrangement to form other types of complexes in solution (Figure 3c–g). To differentiate between the protonated and dissolved states, the SPN coatings dissolved at pH 12 were heated to 90 °C, resulting in a color change from reddish to colorless. UV–vis spectroscopy was also used to analyze the non-heated and heated samples (Figure 3g). The results supported the hydrolysis of the quinone intermediates[43-45] and breakdown of the silicate–quinone structure upon heating, with a peak shift from 325 to 275 nm and the disappearance of band gaps around 400–475 nm and 500–575 nm. This dual pH-responsive disassembly feature offers opportunities to engineer stepwise asymmetric pH responses to environmental stimuli that could potentially occur in environmental or biological applications such wettability changes for oil–water separation, hydrogel actuators, photoswitches, and drug delivery.[42,46-49] For

example, leveraging the dual pH-responsive disassembly of the coatings for the controlled release of fertilizers could provide a dynamic approach to nutrient release in response to soil pH level changes or root exudation with varying pH levels.

2.4. Hydrophobic Functionalization of SPN Coatings

The surface chemistry of the SPN coatings was tuned through post-functionalization with HGs of different lengths to form SPN-HG (HG = PrG, OG, or LG). The gallate groups of these ligands can be coordinated with the preformed Si–TA coating to create a hydrophobic surface (**Figure 4** and Scheme S1). Upon addition of PrG in a mixture of pH 8.5 water/ethanol (1:1, v/v), binding to the preformed SPN layer was observed, as assessed by QCM (Figure 4a, b and Figure S28). Importantly, the resulting $\Delta D/\Delta f$ ratio (where ΔD is dissipation), corresponding to the induced energy loss per unit coupled mass, for regime I was the same as that for regime II ($\Delta D/\Delta f = 0.4 \times 10^{-6}$ Hz^{-1}), indicating that functionalization did not induce disassembly of the existing SPNs (Figure 4c). The high stability of resulting coatings is likely due to (1) the coordination between catecholate silicate complexes of the SPN coatings with catechol groups of the hydrophobic gallates (Figure 4b), (2) the interactions (e.g., π–π stacking and hydrogen bonding) between TA and hydrophobic phenolic ligands, and (3) the entanglement of long alkyl chain of hydrophobic gallates within the pores of the preformed SPN coatings. In addition, longer hydrophobic gallates resulted in higher deposited masses (Figure 4d). The presence of –C–H stretching vibrations in the range of 2800–2970 cm^{-1} in the FTIR spectra of SPN-HGs further confirmed post-functionalization of the SPN coatings (Figure 4e).

Hydrophobic urea@SPN-HG, obtained after post-synthesis functionalization, displayed rougher surface morphologies than urea@SPN (Figure 4f–i). Specifically, functionalization resulted in the uniform growth of rod-like structures on the surface of urea@SPN, where the size of the rods could be adjusted from the micro- to the nanoscale by increasing the length of the alkyl chain in the hydrophobic gallates. These rod-like structures can trap a large volume of tightly packed air bubbles between them (Figure 4b, inset), which is expected to help retain nutrients within urea@SPN granules.[37] The normalized color map obtained through micro-CT scans of urea@SPN-LG indicated a relatively less dense coating than that in urea@SPN, confirming the existence of packed air bubbles (Figure 4j). Water contact angle (WCA) measurements indicated that the degree of hydrophobicity increased as the alkyl chain length of the hydrophobic gallate was extended, resulting in a WCA increase from 20 to 82° (Figure

4k and Figure S29). Cross-sectional SEM images revealed negligible differences in thickness between the pristine SPN coatings and the post-functionalized SPN-HG coatings (Figure 4l and Figure S30). Tuning the surface morphology and hydrophobicity of SPN coatings through post-functionalization with hydrophobic ligands can provide additional control over the cargo release profile.

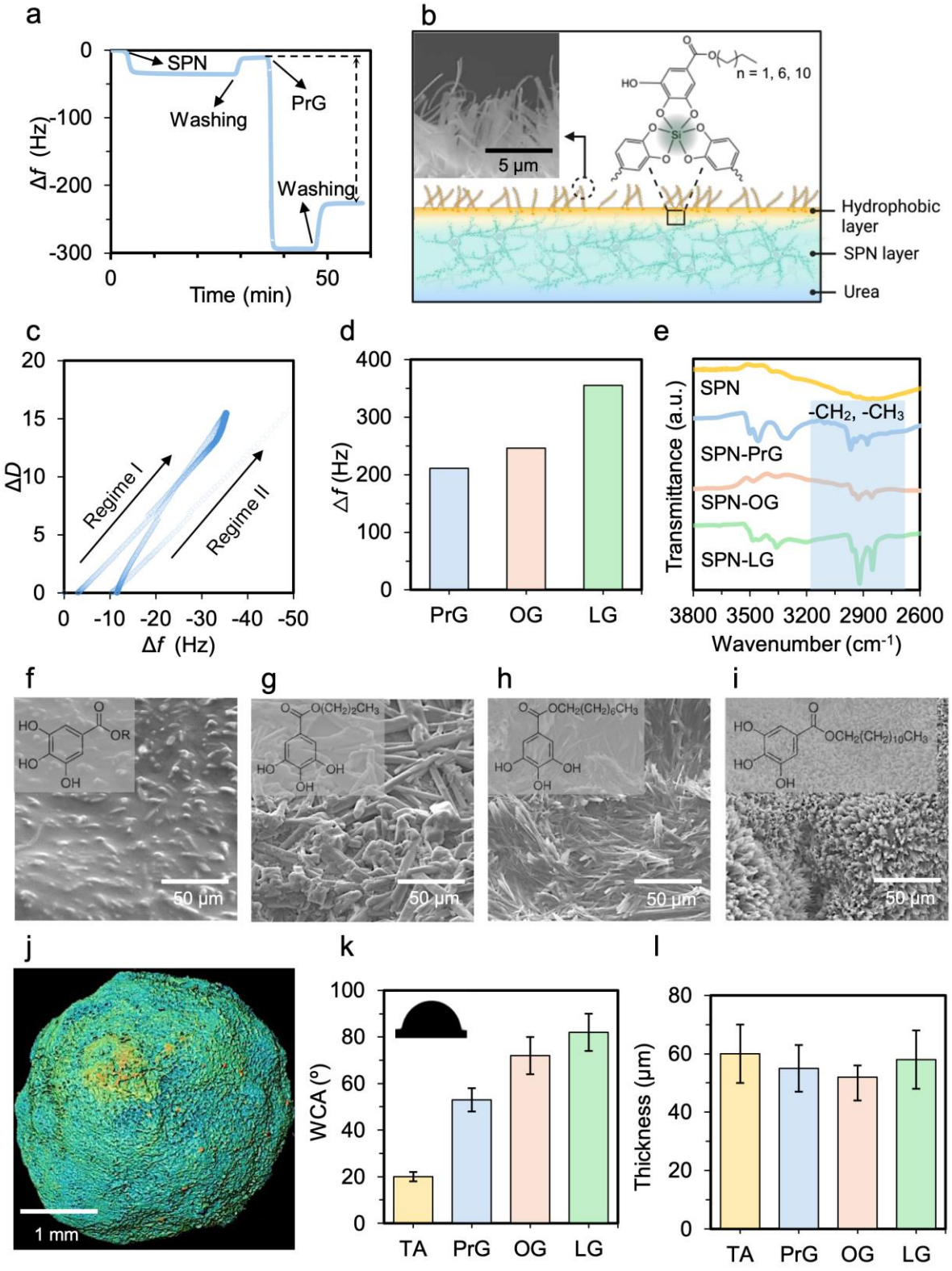

Figure 4. Hydrophobic functionalization of SPN coatings. (a) Binding kinetics of SPN with LG, as measured by QCM. (b) Schematic of the interfacial interactions between the SPN layer and hydrophobic layer (i.e., hydrophobic gallates); inset shows the cross-sectional SEM view of urea@SPN-LG. (c) ΔD–Δf plot illustrating the adhesion dynamics between SPN and LG. Regime I represents the dynamic adsorption of SPN coatings onto the QCM chip. Regime II represents the dynamic adsorption of LG onto the SPN coatings. (d) Frequency shifts upon deposition of hydrophobic gallates on SPN coating. (e) FTIR spectra and (f–i) SEM images of SPN coatings with TA (f) and functionalized with different hydrophobic gallates (g–i). (j) Micro-CT image of urea@SPN-LG. (k) WCA of SPN coatings (Si–TA) and SPN coatings functionalized with different hydrophobic gallates. The inset in (k) shows a water droplet on an SPN-LG coating. (l) Thickness of urea@SPN and urea@SPN functionalized with different hydrophobic gallates, as measured from cross-section SEM images. Three specimens were analyzed for each sample, with the data shown as the mean ± standard deviation, where applicable. Figure 4b was partially created using BioRender.

2.5. SPNs for the Controlled Release of Urea

Polyphenol-based coatings have recently been used in agricultural applications. For example, we reported a strategy for the self-assembly of MPNs on urea granules in organic solvents for application as a controlled release system.[37] Here, we examined the release profile of urea from urea@SPN and urea@SPN-HG in soils as an example of encapsulation using SPN coatings for controlled-release fertilizers (**Figure 5** and Scheme S2). The SNP-coated urea granules with different compositions all showed prolonged urea release profiles lasting up to 10 days, whereas pure urea dissolved completely within a few hours,[50] confirming that SPNs can be effectively used as sustainable coatings for controlled release. Specifically, the release profile of urea could be tuned from 3 to 10 days by varying the molar ratio of Si:TA (Figure S31). The release profile could also be tuned by leveraging the pH responsiveness of the coatings. Complete release of urea in acidic and alkaline soils occurred within 3 and 7 days, respectively, which was faster than that achieved in neutral soils (Figure 5a). Therefore, the release of urea is triggered by the different soil pH levels. Extending the urea release profile is being investigated to prolong the period between the initial application of urea and the first release, with the triggered release mechanism highlighted therein.[51,52] The number of SPN coatings (i.e., the thickness of the coatings) also influenced the release profile of the urea@SPN samples (Figure 5b). Urea release from urea@SPN prepared using 3 SPN deposition cycles (one deposition cycle consists of 10 deposition steps, with each step

involving the application of 0.1 mL of Si–TA solution, totaling 1 mL per cycle) was more sustained than that from urea@SPN prepared with one SPN deposition cycle. The release was further tuned from the hydrophilicity/hydrophobicity of the coating. For instance, urea@SPN-LG demonstrated complete release of urea within 14 days, with less than 50% of urea being released in the first 7 days, highlighting a more sustained release profile than that obtained by hydrophilic urea@SPN (Figure 5c). These results suggest that the density, thickness, and hydrophobicity of the coatings influence the release profile of urea in soils, where the adjustable architecture of the SPN coatings offers potential for practical applications.[50,53,54] For example, prolonging the urea release up to several months could be possibly achieved by using macromolecular conjugated catechol building blocks to engineer SPN coatings.[55-58]

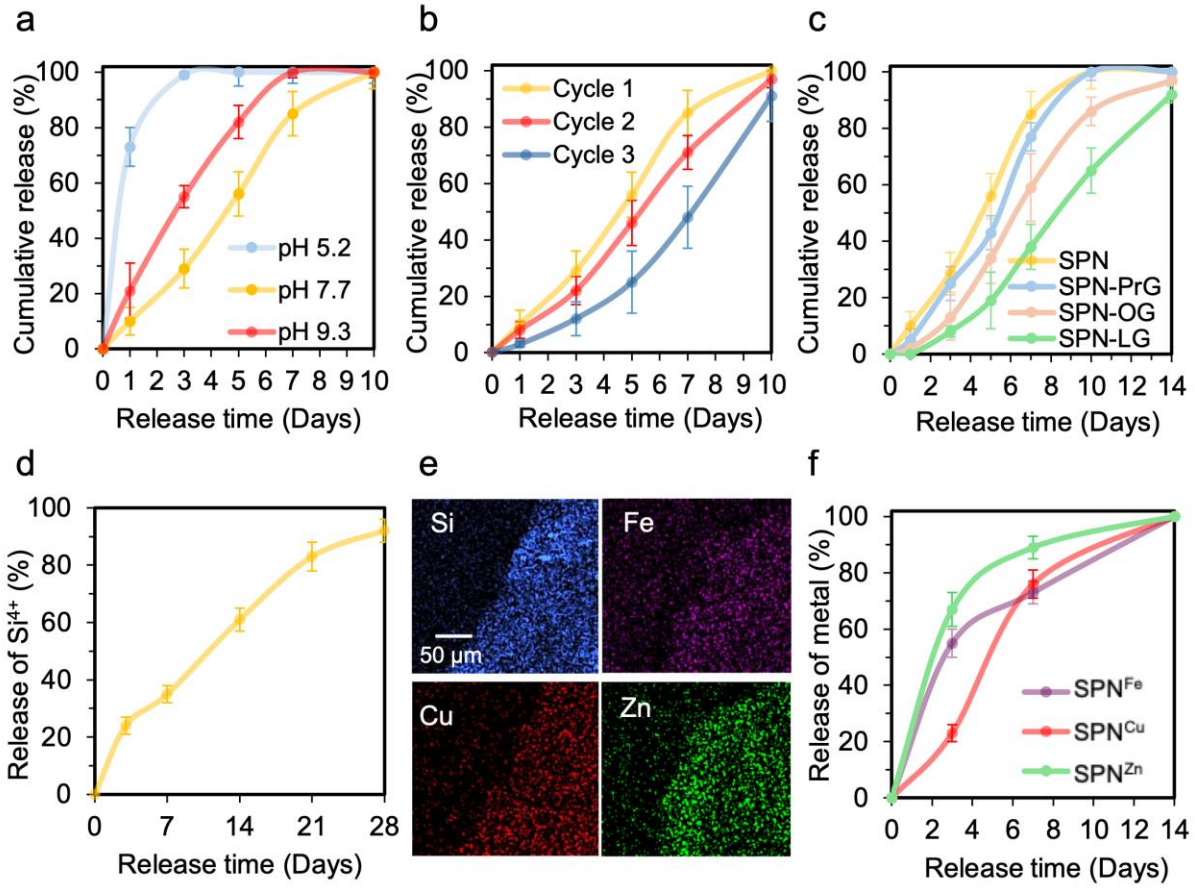

Figure 5. Application of urea@SPN and urea@SPN-HG as controlled-release fertilizers. (a) Cumulative release of urea from urea@SPN at different pH levels of soils at 25 °C. (b, c) Cumulative release rate urea from urea@SPN samples prepared using different deposition cycles (b) and functionalized with different hydrophobic gallates (c). (d) Cumulative release of Si^{4+} from SPN coatings in soil. (e) EDS images of urea@SPN samples post-functionalized with different metal ions. (f) Cumulative release of metal ions in soil from urea@SPN samples functionalized with different metal ions. Release was measured by a colorimetric

method for urea and ICP for Si and metal ions. Data are shown as the mean ± standard deviation, and three specimens were analyzed for each sample.

SPN coatings are also promising for the controlled release of Si^{4+} and micronutrients (e.g., Fe^{3+}, Cu^{2+}, and Zn^{2+}), which are key elements in fertilizers. For example, Si^{4+} in soil plays an essential role in increasing the growth rate of plants, boosting crop productivity, providing protection against a wide range of pathogenic invasions, and enabling adaptation in unfavorable environmental conditions.[59] Specifically, the release of Si^{4+} from the SPN coatings of urea@SPN in soil could be sustained over 28 days (Figure 5d). Furthermore, urea@SPN was post-functionalized with Fe^{3+}, Cu^{2+}, or Zn^{2+} through a dip coating process in ethanol to form urea@SPN^{Fe}, urea@SPN^{Cu}, and urea@SPN^{Zn} (Scheme S3), respectively. The presence of metal ions was confirmed by SEM-energy-dispersive X-ray spectroscopy (EDS) and XPS (Figure 5e and Figure S32).[60,61] As observed from Figure 5f, ~90% of Zn^{2+} were released within 7 days, whereas the release of Cu^{2+} was more sustained, with ~75% released within the same period. Complete release of micronutrients for all metal ions was observed by day 14. In contrast, under the same conditions examined as a control experiment, complete dissolution of metal ions Cu^{2+}, Zn^{2+}, and Fe^{3+} present in free form in soil occurred in less than 4 hours (Figure S33). The variation in the metal release profiles may be attributed to differences in the coordination type and strength of the metal ions with the SPNs. Moreover, ion exchange between metal ions and silicon was detected through XPS analysis, highlighting the coordination of metals ions with phenolic ligands (see the discussion in Figure S32).

3. Conclusion

This work provides insights into the dynamic covalent coordination of SPNs for engineering robust coatings with tunable functionality and controllable disassembly. The chemical composition and aging of the silicate–phenolic solutions significantly influenced the complexation states of the SPNs, while multiple coating steps allowed for thickness control up to 60 μm. Compositional versatility was demonstrated using a wide range of phenolic ligands (i.e., TA, GA, and PG), different substrates (i.e., planar Au, polystyrene nanoparticle, and urea granule), and different metal dopants (i.e., Fe^{3+}, Cu^{2+}, and Zn^{2+}). Furthermore, post-functionalization with phenolic ligands containing long alkyl chains allowed for the hydrophobicity of the SPN coatings to be controlled from 20–82°. Importantly, the SPN coatings feature pH responsiveness (disassembly at pH < 5 and pH > 10), which allows for the stepwise release of urea in soils with different pHs. Specifically, urea encapsulated in the

core could be consistently released over 14 days, whereas micronutrient ions incorporated into the SPN shell could be released over 28 days for Si^{4+} and 14 days for metal ions (Fe^{3+}, Cu^{2+}, Zn^{2+}). The diverse interfacial interactions of the Si–TA coatings are expected to afford the use of SPNs and metalloid–phenolic coatings as versatile platforms, potentially for drug delivery, antifouling and antibacterial applications, food packaging, and insulator coatings in electronic applications.

Supporting Information

Supporting Information is available from the Wiley Online Library or from the author.

Acknowledgements

This research was supported under the Australian Research Council's Industrial Transformation Research Program funding scheme IH200100023. F.C. acknowledges the award of a National Health and Medical Research Council Leadership Fellowship (Grant no. GNT2016732). Z.L. acknowledges The University of Melbourne for an Early Career Researcher grant. A.Z. acknowledges support through the ARC Discovery Early Career Researcher Award (DE240100743) scheme. J.J.R. is recipient of an ARC Future Fellowship (Project no. FT210100669) funded by the Australian Government. We thank the Melbourne Trace Analysis for Chemical, Earth, and Environmental Sciences (TrACEES) Platform for access to the micro-CT scanner and Dr. Jay Black (School of Earth Sciences, The University of Melbourne) for technical assistance with the micro-CT analyses. This work was performed in part at Chemical and Biochemical Engineering Platform, Materials Characterisation and Fabrication Platform (MCFP), and Mass Spectroscopy and Proteomics Facility at Bio21 institute at The University of Melbourne. This research was undertaken in part on the SAXS/WAXS beamline at the Australian Synchrotron, part of ANSTO (Grant No. 18766). We thank Dr. Roya Khalil from Incitec Pivot Limited and Prof. Deli Chen from The University of Melbourne for helpful discussions on industrial concepts of the work. Scheme 1, Figure 3f, Figure 4b, and Scheme S1–S3 were created with BioRender.

Conflict of Interest

The authors declare no competing financial interests.

Received: ((will be filled in by the editorial staff))
Revised: ((will be filled in by the editorial staff))
Published online: ((will be filled in by the editorial staff))

References

[1] H. Furukawa, K. E. Cordova, M. O'Keeffe, O. M. Yaghi, *Science* **2013**, *341*, 1230444.
[2] Z. Lin, J. J. Richardson, J. Zhou, F. Caruso, *Nat. Rev. Chem.* **2023**, *7*, 273–286.
[3] M. A. Rahim, K. Kempe, M. Müllner, H. Ejima, Y. Ju, M. P. van Koeverden, T. Suma, J. A. Braunger, M. G. Leeming, B. F. Abrahams, F. Caruso, *Chem. Mater.* **2015**, *27*, 5825–5832.
[4] W. Xu, Z. Lin, S. Pan, J. Chen, T. Wang, C. Cortez-Jugo, F. Caruso, *Angew. Chem. Int. Ed.* **2023**, *62*, e202312925.
[5] A. Rosenheim, O. Sorge, *Ber. Dtsch. Chem. Ges.* **1920**, *53*, 932–939.
[6] D. Hartmann, T. Thorwart, R. Muller, J. Thusek, J. Schwabedissen, A. Mix, J. H. Lamm, B. Neumann, N. W. Mitzel, L. Greb, *J. Am. Chem. Soc.* **2021**, *143*, 18784–18793.
[7] B. Wolff, A. Weiss, *Angew. Chem. Int. Ed.* **2003**, *25*, 162–163.
[8] D. W. Barnum, *Inorg. Chem.* **1972**, *11*, 1425–1429.
[9] J. J. Flynn, F. Peter Boer, *J. Am. Chem. Soc.* **1969**, *91*, 5756–5761.
[10] D. J. McCord, J. H. Small, J. Greaves, Q. N. Van, A. J. Shaka, E. B. Fleischer, K. J. Shea, *J. Am. Chem. Soc.* **1998**, *120*, 9763–9770.
[11] S. Bai, Y. Tsuji, Y. Okaue, T. Yokoyama, *Chem. Lett.* **2008**, *37*, 1168–1169.
[12] A. Millanvois, C. Ollivier, L. Fensterbank, *Eur. J. Inorg. Chem.* **2022**, *2022*, e202101109.
[13] V. Campisciano, B. Taormina, A. Spinella, L. F. Liotta, F. Giacalone, M. Gruttadauria, *Molecules* **2022**, *27*, 2521–2532.
[14] S. Oshaghi, *J. Chromatogr. A* **2024**, *1729*, 465016.
[15] E. P. Kramarova, A. D. Volodin, V. V. Negrebetsky, A. D. Shagina, T. M. Aliev, P. V. Dorovatovskii, R. A. Novikov, A. V. Vologzhanina, A. A. Korlyukov, *Molecules* **2021**, *26*, 3548.
[16] S. Escario, M. Nightingale, P. Humez, B. M. Tutolo, *Geochim. Cosmochim. Acta* **2020**, *280*, 185–201.
[17] Z. Diao, L. Li, H. Zhou, L. Yang, *Regener. Biomater.* **2024**, *11*, rbae053.
[18] J. Roeser, D. Prill, M. J. Bojdys, P. Fayon, A. Trewin, A. N. Fitch, M. U. Schmidt, A. Thomas, *Nat. Chem.* **2017**, *9*, 977−982.
[19] O. Yahiaoui, A. N. Fitch, F. Hoffmann, M. Froba, A. Thomas, J. Roeser, *J. Am. Chem. Soc.* **2018**, *140*, 5330−5333.
[20] M. Naoe, H. Iwashita, S. Saito, M. Koike, H. Wada, A. Shimojima, K. Kuroda, *Chem. Lett.* **2020**, *49*, 1075–1077.
[21] V. V. Volkov, T. J. Blundell, S. Argent, C. C. Perry, *Dalton Trans.* **2023**, *52*, 7249–7257.
[22] F. Weber, E. Sagstuen, Q. Z. Zhong, T. Zheng, H. Tiainen, *ACS Appl. Mater. Interfaces* **2020**, *12*, 52457–52466.

[23] F. Weber, W. C. Liao, A. Barrantes, M. Eden, H. Tiainen, *Chemistry* **2019**, *25*, 9870–9874.
[24] F. Weber, A. Barrantes, H. Tiainen, *Langmuir* **2019**, *35*, 3327–3336.
[25] G. S. Pokrovski, J. Schott, *Geochim. Cosmochim. Acta* **1998**, *62*, 3413–3428.
[26] H. Ohsaki, K. Miura, A. Imai, M. Tada, M. A. Aegerter, *J. Sol-Gel Sci. Technol.* **1994**, *2*, 245–249.
[27] J. Duo, Z. Zhang, G. Yao, Z. Huo, F. Jin, *Catal. Today* **2016**, *263*, 112–116.
[28] M. D. Yuniati, T. Hirajima, H. Miki, K. Sasaki, *Mater. Trans.* **2015**, *56*, 1733–1741.
[29] M. K. Vera, J. L. Patrick, in *Proceedings SPIE, Instruments, Methods, and Missions for Astrobiology XI*, Vol. 7097 (Eds: R. B. Hoover, G. V. Levin, A. Y. Rozanov, P. C. Davies), Society of Photo-Optical Instrumentation Engineers (SPIE) **2008**, p. 709706.
[30] Y. Hu, S. J. Teat, W. Gong, Z. Zhou, Y. Jin, H. Chen, J. Wu, Y. Cui, T. Jiang, X. Cheng, W. Zhang, *Nat. Chem.* **2021**, *13*, 660–665.
[31] V. V. Annenkov, E. N. Danilovtseva, V. A. Pal'shin, O. N. Verkhozina, S. N. Zelinskiy, U. M. Krishnan, *RSC Adv.* **2017**, *7*, 20995–21027.
[32] X. Fu, A. Wang, M. J. Krawczynski, *J. Geophys. Res.: Planet* **2017**, *122*, 839–855.
[33] R. Javad Kalbasi, S. Mansouri, O. Mazaheri, *Res. Chem. Intermed.* **2018**, *44*, 3279–3291.
[34] R. Javad Kalbasi, P. Parishani, O. Mazaheri, *J. Cluster Sci.* **2018**, *29*, 561–575.
[35] P. Uznanski, A. Walkiewicz-Pietrzykowska, K. Jankowski, J. Zakrzewska, A. M. Wrobel, J. Balcerzak, J. Tyczkowski, *Appl. Organomet. Chem.* **2020**, *34*, e5674.
[36] T. Wang, Z. Lin, O. Mazaheri, J. Chen, W. Xu, S. Pan, C.-J. Kim, J. Zhou, J. J. Richardson, F. Caruso, *Angew. Chem. Int. Ed.* **2024**, e202410043.
[37] O. Mazaheri, M. S. Alivand, A. Zavabeti, S. Spoljaric, S. Pan, D. Chen, F. Caruso, H. C. Suter, K. A. Mumford, *Adv. Funct. Mater.* **2022**, *32*, 2111942.
[38] D. F. Evans, J. Parr, E. N. Coker, *Polyhedron* **1990**, *9*, 813–823.
[39] Y. Liu, J. Jia, Z. Liu, N. Pu, G. Ye, W. Wang, T. Hu, T. Qi, J. Chen, *Chem. Mater.* **2021**, *33*, 4733–4744.
[40] J. Guo, J. J. Richardson, Q. A. Besford, A. J. Christofferson, Y. Dai, C. W. Ong, B. L. Tardy, K. Liang, G. H. Choi, J. Cui, P. J. Yoo, I. Yarovsky, F. Caruso, *Langmuir* **2017**, *33*, 10616–10622.
[41] S. Quideau, D. Deffieux, C. Douat-Casassus, L. Pouységu, *Angew. Chem. Int. Ed.* **2011**, *50*, 586–621.
[42] Q. Z. Zhong, J. J. Richardson, Y. Tian, H. Tian, J. Cui, S. Mann, F. Caruso, *Angew. Chem. Int. Ed.* **2023**, *62*, e202218021.
[43] P. W. G. Smith, A. R. Tatchell, in *Aromatic Chemistry* (Eds.: P. W. G. Smith, A. R. Tatchell), Pergamon, **1969**, pp. 144–175.
[44] L. Michaelis, *Chem. Rev.* **1935**, *16*, 243–286.
[45] J. B. Conant, L. F. Fieser, *J. Am. Chem. Soc.* **1924**, *46*, 1858–1881.
[46] M. Qu, Y. Pang, J. Li, R. Wang, D. He, Z. Luo, F. Shi, L. Peng, J. He, *Colloids Surf., A* **2021**, *624*, 126817.
[47] Z. Han, P. Wang, G. Mao, T. Yin, D. Zhong, B. Yiming, X. Hu, Z. Jia, G. Nian, S. Qu, W. Yang, *ACS Appl. Mater. Interfaces* **2020**, *12*, 12010–12017.

[48] Y.-Y. Wu, L.-D. Chen, X.-H. Cai, Y. Zhao, M. Chen, X.-H. Pan, Y.-Q. Li, *ACS Appl. Mater. Interfaces* **2021**, *13*, 25241–25249.
[49] J. Dong, W. Chen, J. Feng, X. Liu, Y. Xu, C. Wang, W. Yang, X. Du, *ACS Appl Mater Interfaces* **2021**, *13*, 19507–19520.
[50] O. Mazaheri, A. Zavabeti, R. V. McQuillan, Z. Lin, M. S. Alivand, E. Della Gaspera, D. Chen, F. Caruso, H. Suter, K. A. Mumford, *Chem. Mater.* **2023**, *35*, 7800−7813.
[51] L. Li, G. Bai, W. Gu, C. Niu, Y. Feng, Z. Wei, K. Chen, X. Guo, *Ind. Crops Prod.* **2024**, *221*, 119336.
[52] F. Yang, J. Wang, S. Song, P. Rao, R. Wang, S. Liu, L. Xu, F. Zhang, *J. Agric. Food. Chem.* **2020**, *68*, 7819–7829.
[53] R. V. McQuillan, G. W. Stevens, K. A. Mumford, *ACS Sustain. Chem. Eng.* **2023**, *11*, 122–132.
[54] M. Zhang, Y. Zhang, Y. Yuan, J. Sun, X. Tian, J. Jin, W. Wu, K. Ayikanbaier, *ACS Sustain. Chem. Eng.* **2024**, *12*, 4423-4434.
[55] C. J. Kim, E. Goudeli, F. Ercole, Y. Ju, Y. Gu, W. Xu, J. F. Quinn, F. Caruso, *Angew. Chem. Int. Ed. Engl.* **2023**, *63*, e202315297.
[56] C.-J. Kim, F. Ercole, Y. Ju, S. Pan, J. Chen, Y. Qu, J. F. Quinn, F. Caruso, *Chem. Mater.* **2021**, *33*, 8477–8488.
[57] F. Ercole, C. J. Kim, N. V. Dao, W. K. L. Tse, M. R. Whittaker, F. Caruso, J. F. Quinn, *Biomacromolecules* **2023**, *24*, 387–399.
[58] C. J. Kim, F. Ercole, J. Chen, S. Pan, Y. Ju, J. F. Quinn, F. Caruso, *J. Am. Chem. Soc.* **2022**, *144*, 503–514.
[59] R. Tayade, A. Ghimire, W. Khan, L. Lay, J. Q. Attipoe, Y. Kim, *Biomolecules* **2022**, *12*, 1027.
[60] A. Reyhani, O. Mazaheri, M. Sheikh Alivand, K. Mumford, G. G. Qiao, *Polym. Chem.* **2020**, *11*, 2838–2846.
[61] M. S. Alivand, O. Mazaheri, Y. Wu, A. Zavabeti, G. W. Stevens, C. A. Scholes, K. A. Mumford, *ACS Appl. Mater. Interfaces* **2021**, *13*, 57294–57305.

A strategy is presented to exploit the dynamic covalent coordination of silicate–phenolic networks (SPNs) for coating diverse substrates, allowing the engineering of SPN coatings with different physiochemical properties. The pH responsiveness and tailorable hydrophobicity of the SPN materials allow the controlled release of small molecules, such as fertilizers and micronutrients, making them of interest in agricultural applications and beyond.

O. Mazaheri, Z. Lin, W. Xu, M. Mohankumar, T. Wang, A. Zavabeti, R. V. McQuillan, J. Chen, J. J. Richardson, K. A. Mumford, F. Caruso*

Assembly of Silicate–Phenolic Network Coatings with Tunable Properties for Controlled Release of Small Molecules